PERGAMON

Atmospheric Environment 36 (2002) 4251–4264

ATMOSPHERIC ENVIRONMENT

www.elsevier.com/locate/atmosenv

# Transfer of reactive nitrogen in Asia: development and evaluation of a source–receptor model

Tracey Holloway[a,*], Hiram Levy II[b], Gregory Carmichael[c]

[a] *Columbia Earth Institute, Columbia University, New York, NY 10027, USA*
[b] *NOAA Geophysical Fluid Dynamics Laboratory, Princeton, NJ 08542, USA*
[c] *Department of Chemical and Biochemical Engineering, Center for Global and Regional Environmental Research, The University of Iowa, IA 52242, USA*

Received 2 January 2002; accepted 24 April 2002

**Abstract**

A simple model of chemistry and transport, ATMOS-N, has been developed to calculate source–receptor relationships for reactive nitrogen species within Asia. The model is intended to support discussion of energy and environmental issues in Asia, to compare sulfate and nitrate contributions to regional acidification, and to estimate how each nation's acid deposition and air quality relates to domestic versus foreign emissions. ATMOS-N is a Lagrangian "puff" model in which non-interacting puffs of emissions are advected horizontally and mixed between three vertical layers. Results are compared with wet nitrate deposition observations in Asia.

On an annual average, the model estimates that long-range transport contributes a significant percentage of total nitrate deposition throughout east Asia. China, the largest emitter of the region, contributes 18% to nitrate deposition in Taiwan, 18% in Japan, 46% in North Korea, and 26% in South Korea. South Korea contributes 12% to nitrate deposition in Japan, due to its close upwind proximity. Compared with total acid deposition (nitrate + sulfate), nitrate contributes 30–50% over northern Japan, 30–60% in India, and 50–90% in southeast Asia where biomass burning emits high levels of $NO_x$. The percentage contribution of nitrate is very low in China, where emissions and deposition of sulfur are extraordinarily high.


*Keywords:* Acid deposition; Asia; Lagrangian models; Pollution; Transboundary

## 1. Introduction

Although a number of models have been used to estimate the transport of sulfur species ($SO_2$, $SO_4^{2-}$) within Asia, to date, the regional exchange of nitrogen species has received relatively little attention. Nitrate ($NO_3^-$), a product of emitted nitrogen oxides ($NO_x$), has been shown to contribute 1/3 or more of total acidification through much of Japan (Fujita et al., 2000). This contribution is expected to grow as the transport sector in Asia expands, and as $NO_x$ emission controls lag $SO_2$ emission controls through much of the region.

The present study calculates the exchange of reactive nitrogen species within Asia, the so-called "source–receptor" relationships (SRRs), using a relatively simple model, "ATMOS-N". ATMOS-N is a Lagrangian "puff" model in which non-interacting puffs of emissions are advected horizontally and mixed between three vertical layers. By SRR we refer to the quantitative relationship connecting a unit of emissions from one region to the deposition or concentration of odd-nitrogen species in other regions.

Our study is motivated by the need for modeling tools to support policy decisions related to the transport of air pollution on regional and global scales. The research in

*Corresponding author. Fax: +1-212-854-6309.
*E-mail address:* th2024@columbia.edu (T. Holloway).

1352-2310/02/$ - see front matter 
PII: S1352-2310(02)00316-3

some respects parallels the development of the European Monitoring and Evaluation Program (EMEP) chemical transport model. As a component of integrated assessment analysis for Europe, the EMEP model provided support for designing protocols to the 1979 Convention on Long Range Transboundary Air Pollution and recent directives of the European Union. Policy options in Europe were explored with the help of the Regional Air Pollution Information and Simulation (RAINS)-Europe integrated assessment model (e.g. Alcamo et al., 1990). RAINS-Europe used SRRs calculated by the EMEP model of atmospheric chemistry and transport (e.g. Eliassen, 1978; Simpson, 1992; Barrett et al., 1995). Just as the EMEP model provides atmospheric transport and deposition input to RAINS-Europe, so has the sulfur version of ATMOS supported the development of the RAINS-Asia model (e.g. Foell et al., 1995). By expanding the capabilities of ATMOS to address odd-nitrogen species (through ATMOS-N), control options for $NO_x$ emissions, and the environmental effects of different policies, may be analyzed in a framework consistent with ongoing analysis of $SO_2$ options and impacts in Asia.

The choice of ATMOS-N for this modeling study fulfills multiple objectives: (1) It allows the examination of nitrate transport and deposition within a framework comparable with that used for sulfate deposition in previous ATMOS studies (e.g. Calori et al., 2001); (2) the calculation of annual, detailed source–receptor matrices can be performed much more expediently than with an Eulerian model of the same resolution; and (3) by exploring the performance of ATMOS-N, the advantages and limitations of simple models may be better evaluated.

ATMOS-N is a version of the ATMOS model designed to simulate reactive nitrogen species. ATMOS has been used in a number of studies examining sulfur transport and deposition in Asia. The model has been used to assess impacts of sulfur emissions on a sectoral basis in the context of the RAINS-Asia policy assessment model (Arndt et al., 1997), to examine the sulfur budget and sulfur deposition pathways (Xu and Carmichael, 1999), and to study the seasonal and interannual behavior of sulfur species in Asia (Guttikunda et al., 2001; Calori et al., 2001). Applied to urban scales as the UR-BAT model, ATMOS addressed transport and diffusion of sulfur species in Beijing and Bombay (Calori and Carmichael, 1999).

Other models have also addressed regional exchange of pollutants in Asia. Sulfur has by far been the most widely studied species, due to its high level of emissions, importance in acidification, associated health risks, and relatively simple chemistry (e.g. Huang et al., 1995; Ichikawa and Fujita, 1995; Kotamarthi and Carmichael, 1990). The growing field of models addressing sulfur transport in east Asia has not produced a convergence of results. In considering the contribution of sulfur emissions from China to sulfate deposition in Japan, for instance, estimates range from 3.5% (Huang et al., 1995) to about 45% (Ichikawa and Fujita, 1995).

Relatively little work has been done modeling reactive-nitrogen species in Asia, with some regional exceptions (e.g. Kitada et al., 1993; Wang et al., 2002), and a number of global studies addressing $NO_y$ chemistry in Asia from a global perspective (e.g. Levy et al., 1999; Horowitz and Jacob, 1999). However, no group has yet calculated SRRs for nitrogen species in Asia.

Other atmospheric species in Asia have been investigated with both global and regional models, including tropospheric ozone (e.g. Ueda and Carmichael, 1995; Carmichael et al., 1998; Chameides et al., 1999; Mauzerall et al., 2000); non-methane hydrocarbons (NMHCs) (Phadnis and Carmichael, 2000); and soil aerosols (Wang et al., 2002). Growing interest is also focussing on the hemispheric and global impacts of emissions from Asia (e.g. Jaffe et al., 1999; Berntsen et al., 1999; Jacob et al., 1999; Yienger et al., 2000).

## 2. ATMOS-N model structure

The model employed for this study is ATMOS-N, a three-layer Lagrangian "puff" model solving atmospheric chemistry and transport on a regional basis. ATMOS has evolved from the National Oceanic and Atmospheric Administration (NOAA) Branching Atmospheric Trajectory (BAT) model (Heffter, 1983), originally designed as a multi-purpose tracer model. Prior to the current study, only sulfur chemistry has been included in ATMOS. (Foell et al., 1995; Arndt et al., 1998; Calori and Carmichael, 1999; Streets et al., 1999).

In ATMOS, emissions are modeled as non-interacting puffs that are advected horizontally and split in the vertical, simulating mixing due to vertical wind shear (three layers at night, two during the day). Splitting is triggered by alterations in the boundary layer height and by night-to-day and day-to-night transitions, when the number of model layers changes. After a puff splits, it is assumed that the new puff mass mixes uniformly through the thickness of each layer. The vertical mixing mechanism does not account for direct vertical motion, such as convection or frontal passages. This parameterization of vertical motion is the model's most drastic simplification.

As puffs move away from their emission source, they grow, reflecting the horizontal spreading of the puffs in an assumed Gaussian plume. To calculate concentration and deposition (given below), an exponential mass drop-off is assumed from the puff center, and the radius of each puff grows linearly in time at a rate of $0.5\,m\,s^{-1}$ (with initial radii of 40 km for area emissions

and 10 km for large point sources). Output fields of concentration and deposition are calculated by summing the contributions of individual parcels onto each grid box.

Emissions input and concentration/deposition output are given on a 1° × 1° grid over the model domain, from 60°E to 150°E and 20°S to 50°N. Emissions are modeled as "puffs" of $NO_x$ ($NO + NO_2$), released every 3 h into the model. The top of the nighttime surface layer is 300 m, the top of the mixed boundary layer is variable (up to 2500 m), and the top of the free troposphere in the model is 6000 m.

Six-hour average horizontal winds and precipitation (2.5° × 2.5° resolution) from National Centers for Environmental Prediction (NCEP) reanalysis data are used to calculate horizontal advection and wet deposition. Simulations discussed here were performed with 1990 NCEP fields (see Figs. 1 and 2).

ATMOS only advects and transforms species within active puffs, so the computational costs scale with the number of emission sources. To calculate the SRRs, the model is run many times, with each simulation including emissions from a single gridbox. Given the scalability of ATMOS, running these multiple single-source simulations is computationally very efficient.

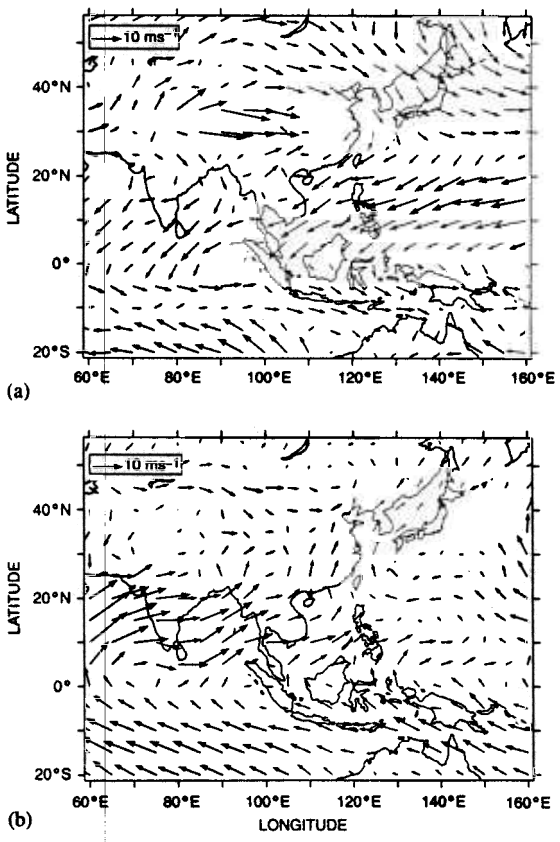


Fig. 1. (a) January average winds in the model-defined boundary layer from NCEP reanalysis; and (b) same, for July.

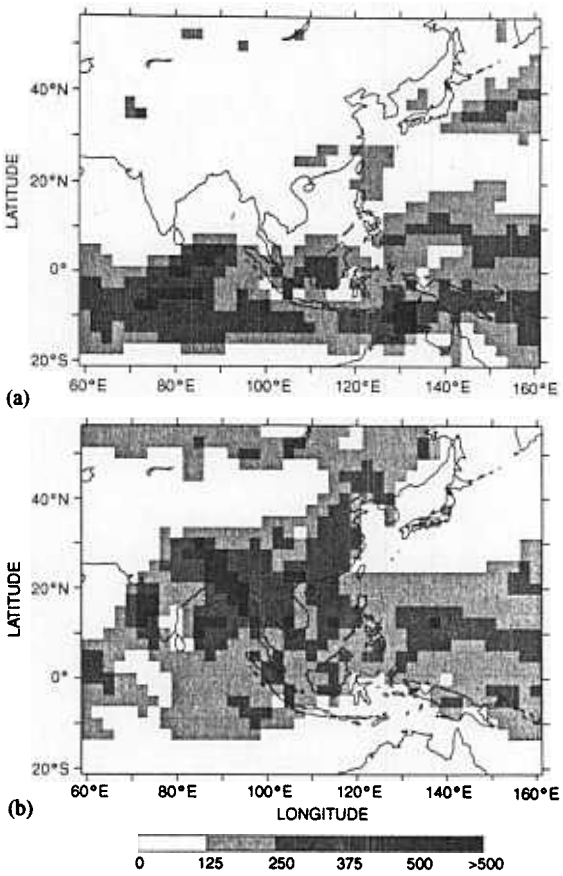


Fig. 2. (a) January precipitation from NCEP reanalysis (mm/month) and (b) same, for July.

### 2.1. Emissions

$NO_x$ emissions over the model domain are included from fossil fuel burning, biomass burning, and biogenic soil emissions, which sum to 7850 kton N $yr^{-1}$ (25.8 Tg $NO_2$ $yr^{-1}$). Fossil fuel emissions are taken from the latest estimates from the International Institute for Applied Systems Analysis (IIASA) (Klimont, 2001), as well as estimates from van Aardenne et al. (1999) over regions for which IIASA estimates are unavailable. Merging the two fossil fuel estimates yields total 1990 emissions of 5170 kton N $yr^{-1}$ (17.0 Tg $NO_2$ $yr^{-1}$), 88% from regional sources and 12% from large point sources (Fig. 3). National fossil fuel emissions for Taiwan, Japan, North Korea, South Korea, China and India are presented in Table 1. Fossil fuel emissions are assumed to have no seasonal cycle. Because acid

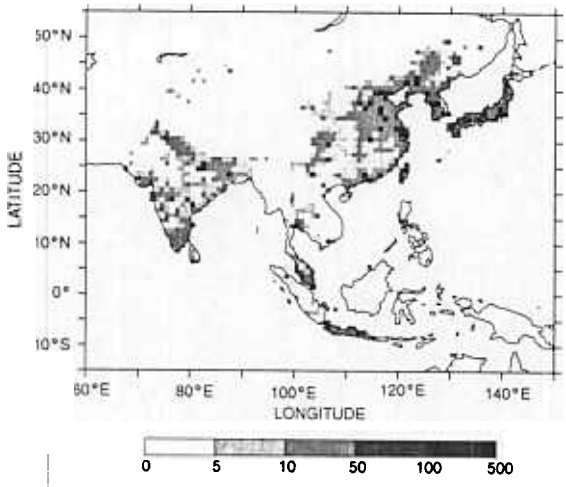


Fig. 3. Annual average emissions from fossil fuel burning (kton N gridbox$^{-1}$ yr$^{-1}$).

Table 1
Estimates of annual fossil fuel emissions in units kton N yr$^{-}$
No seasonality is assumed

| Country | Emissions (kton N yr$^{-1}$) |
|---|---|
| an | 116 |
| | 556 |
| Korea | 120 |
| Korea | 256 |
| | 2132 |
| | 1020 |

deposition—a cumulative process—is the primary focus of this work, seasonal variations in fossil fuel emissions are not viewed as a large source of error.

Annual emissions from biomass burning and biogenic sources are 1520 kton N (5.0 Tg $NO_2$) and 1160 kton N (3.8 Tg $NO_2$), respectively, with monthly variations. The biomass burning source is taken from Galanter et al. (2000), with a reduction in summertime burning in east Asia based on more recent analysis. Figs. 4a and b show January and July biomass burning emission patterns. Estimated burning in southeast Asia occurs in the winter and spring, peaking in March. Estimated burning in the mid-latitudes occurs from June to September. This estimate includes forest, savanna, and agricultural residues (biofuels are included in the fossil fuel total). The biogenic emissions source is from Yienger and Levy (1995). Figs. 5a and b show biogenic emission patterns. In winter months, growth of emitting foliage is confined to tropical regions; in summer, high emission levels are estimated throughout the domain.

Rather than calculating emissions from all sources, only those $>0.6$ kton N (2 kton $NO_2$) yr$^{-1}$ gridbox$^{-1}$ ($1° \times 1°$) are considered. Because computational require-

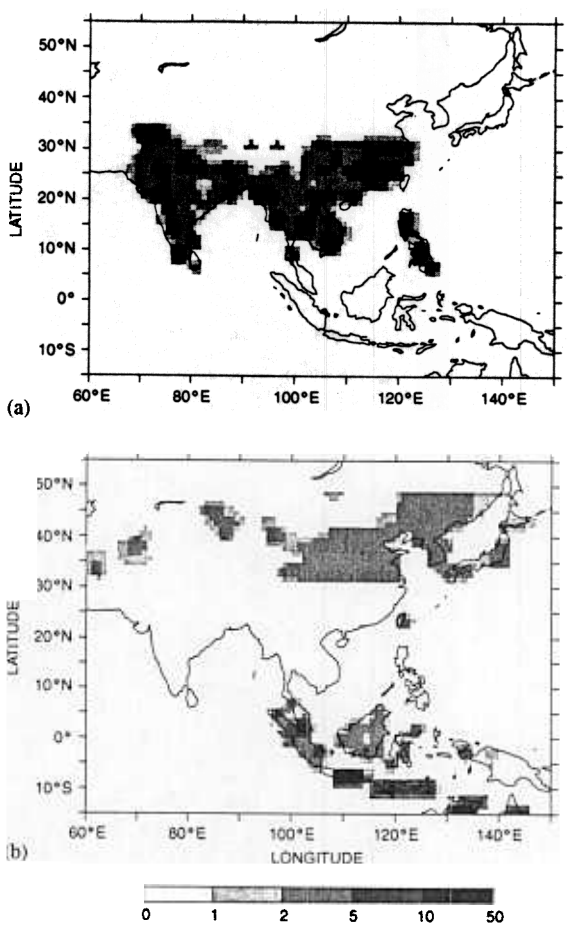


Fig. 4. (a) January emissions from biomass burning (kton N gridbox$^{-1}$ yr$^{-1}$) and (b) same, for July.

ments scale (almost) linearly with the number (but not the strength) of emission sources, this cut-off reduces computing requirements by 55% while only neglecting 5% of the emitted mass.

### 2.2. Chemistry implementation

Three species are carried in ATMOS-N: nitrogen oxides ($NO_x = NO + NO_2$), peroxyacetylnitrate (PAN, $CH_3C(O)O_2NO_2$), and nitric acid ($HNO_3$). $NO_x$ is the only emitted species; PAN is the most stable of the three compounds at low temperatures, and plays an important role in long-range transport; $HNO_3$ is the acidifying species which experiences both wet and dry deposition. These three species are collectively referred to as "odd-nitrogen" species, or $NO_y$ (where $NO_y = NO_x + PAN + HNO_3$).

The method of estimating $NO_y$ chemistry in ATMOS has been adopted from the Global Chemical Transport

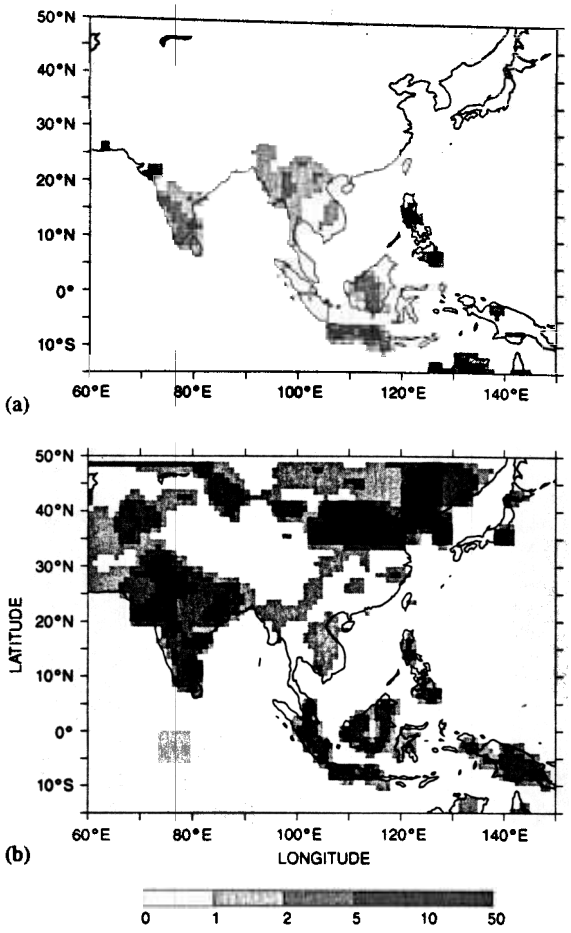


Fig. 5. (a) January emissions from biogenic sources (kton N gridbox$^{-1}$ yr$^{-1}$) and (b) same, for July.

Model developed at the NOAA Geophysical Fluid Dynamics Laboratory (GFDL GCTM) (Kasibhatla et al., 1991; Klonecki, 1998; Levy et al., 1999). The approach was selected as a computationally efficient means of solving for the interconversions of $NO_x$, PAN, and $HNO_3$, without needing to calculate the many species involved in the full chemistry of odd-nitrogen compounds in the atmosphere. Reaction rates in the reduced chemical scheme depend on background concentrations of OH, $HO_2$, NO and $NO_2$. These values are interpolated from pre-calculated, monthly mean, zonally averaged tables generated with a box model solving the carbon monoxide (CO)—methane ($CH_4$)—odd-nitrogen ($NO_y$)—water vapor ($H_2O$)—ozone ($O_3$) mechanism, based on specified monthly mean fields of $NO_x$, CO, $CH_4$, non-methane hydrocarbons, $O_3$, $H_2O$, temperature, and pressure.

Although $HNO_3$ exists as both a gas and aerosol, ATMOS-N does not distinguish between the two forms. Fractionation between gas and aerosol is approximated in specifying the dry deposition velocities. Over the ocean a greater fraction of $HNO_3$ exists in aerosol form, which has a slower rate of dry deposition. Thus, the dry deposition velocity of $HNO_3$ is much less over ocean than over land. This land–sea breakdown would not capture additional variations in dry deposition velocities, such as where a high fraction of $HNO_3$ has been converted to aerosol due to reactions with ammonia. We note that it is one of the many uncertainties associated with the dry deposition parameterization in the model (see the next section).

As implemented in the GFDL GCTM, this mechanism has produced realistic fields, e.g. for wet $HNO_3$ deposition, the model agrees with regional measurements within $\pm 50\%$ at $\sim 87\%$ of Asian and remote sites (Levy et al., 1999).

### 2.3. Dry and wet deposition

Deposition—both dry and wet—is the only mechanism removing reactive nitrogen from a puff. All three species ($NO_x$, PAN and $HNO_3$) undergo dry deposition, but only $HNO_3$ is soluble and therefore subject to wet deposition.

Dry deposition is implemented in a method parallel to that used in the sulfur version of ATMOS, using the same deposition velocities as the GFDL GCTM (Kasibhatla et al., 1993 and references therein). These deposition velocities are applied to species in the lowest model layer based on latitude, land-cover, and month ($HNO_3$ deposition velocities range 0.3–1.5 cm s$^{-1}$; $NO_x$, 0–0.25 cm s$^{-1}$; PAN, 0–0.25 cm s$^{-1}$).

The wet deposition scavenging rate is calculated using precipitation from the NCEP reanalysis data. The form of the $HNO_3$ deposition function is the same as that used for $SO_4^{2-}$ deposition in ATMOS, based on empirical evaluation of wet sulfate removal in recent model studies (Calori and Carmichael, 1999, and references therein). A uniform precipitation rate is applied to all model layers, and removal scales as the precipitation raised to the 0.83 power.

## 3. Comparison with observations

Comparing model results with measurements yields the most intuitive and most valuable means of model evaluation. However, even measured data contain errors and inconsistencies. Plus, only a limited number of model output variables are measurable, or measurable in a way directly comparable with the model output. Here nitric acid wet deposition is the primary variable for comparison. (For additional comparison with upper and lower level $NO_x$ concentrations over regions in the western Pacific from PEM-West A and B, see Holloway, 2001).

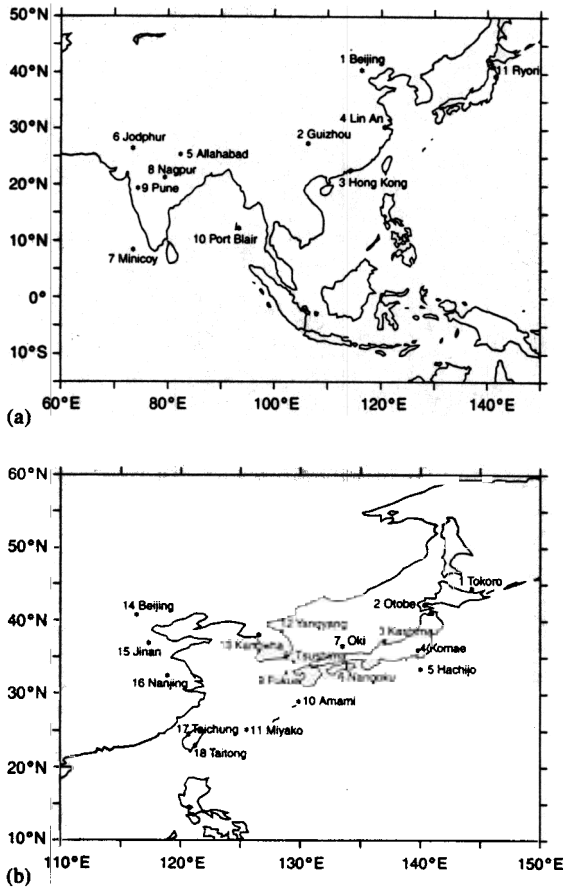


Fig. 6. (a) Locations of DC94 observation sites and (b) locations of Fujita et al. (2000) observation sites.

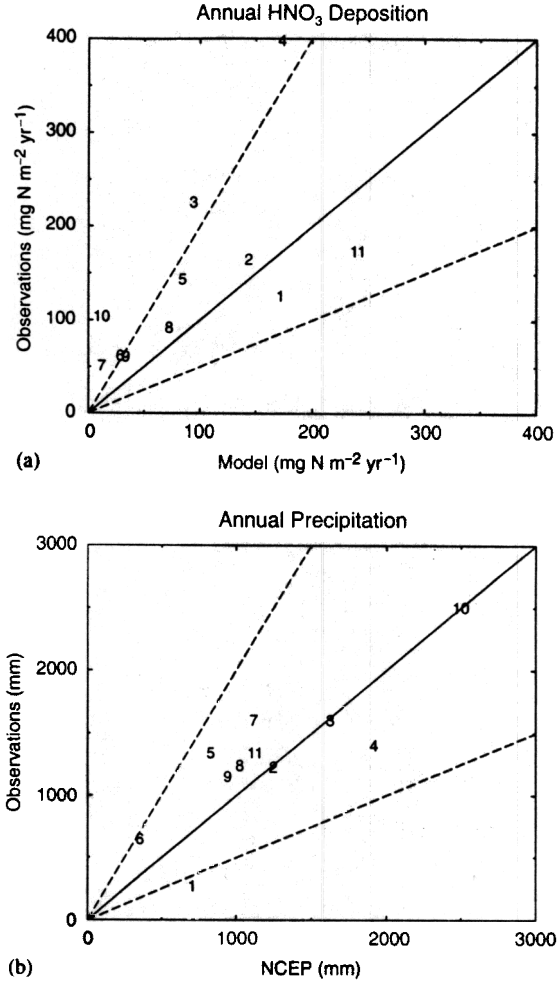


Fig. 7. Comparison of $HNO_3$ wet deposition (a) and precipitation (b) between ATMOS-N and DC94 measurements. Each point represents a DC94 observing station, with indices given in Fig. 6a.

Dentener and Crutzen (1994) provide a data set (hereafter referred to as "DC94") including annual average wet $HNO_3$ deposition values at 11 sites measured by Galloway et al. (1987) and WMO (1993), compiled over a number of years (e.g. Beijing and Guizhou measurements are from 1984). Fig. 6a shows the locations of these sites, which generally cover India fairly well, China sparsely, and include one site in Japan. Wet deposition values calculated by ATMOS-N are compared with those from the DC94 data set in Fig. 7a, and precipitation values are compared with DC94 in Fig. 7b. Note that model precipitation is similar to NCEP reanalysis precipitation, which are similar to the DC94 values (See Table 2 for regression statistics).

The second data set for comparison is that presented by Fujita et al. (2000). The 18 Fujita et al. sites are concentrated in Japan, Korea, and eastern China (Fig. 6b), regions where DC94 has few sites. Furthermore, the Fujita et al. (2000) data are given by season, allowing an examination of model seasonality. Data were collected between June 1992 and May 1993. Following the convention of Fujita et al. (2000), only two seasons are considered: summer (June–September) and "non-summer" (October–May).

The comparisons of both data sets with ATMOS-N exhibit low bias in simulated wet $HNO_3$. In both data sets, the easternmost monitoring stations have a higher tendency toward model underestimation. Model underestimation of wet deposition is most pronounced in the summer season (Fig. 8a). To eliminate the effect of bias in precipitation between the model and the Fujita et al.'s (2000) observations, we also compare concentration (Figs. 8c, 9c and 10c). The low bias persists in the comparison of concentrations, suggesting that differences in precipitation alone do not explain the model's lower deposition values.

Table 2
Regression statistics for all measurement–observation comparisons

| Figure # | Description | Y-intercept | Slope | $R^2$ |
|---|---|---|---|---|
| 1a | DC94 wet $HNO_3$ deposition | | | 0.37 |
| 1b | DC94 precipitation | | | 0.72 |
| 2a | Fujita et al., summer wet $HNO_3$ deposition | | | 0.59 |
| 2b | Fujita et al., summer precipitation | | | 0.03 |
| 2c | Fujita et al., summer wet $HNO_3$ concentration | | | 0.44 |
| 3a | Fujita et al., non-summer wet $HNO_3$ deposition | | | 0.18 |
| 3b | Fujita et al., non-summer precipitation | | | 0.55 |
| 3c | Fujita et al., non-summer wet $HNO_3$ concentration | | | 0.78 |
| 4a | Fujita et al., annual wet $HNO_3$ deposition | | | 0.53 |
| 4b | Fujita et al., annual precipitation | | | 0.14 |
| 4c | Fujita et al., annual wet $HNO_3$ concentration | | | 0.69 |

A number of factors may be responsible for the model's low estimates of $HNO_3$ deposition. The precipitation or wind fields may be incorrect, either because the 1990 simulation year does not adequately represent the years in which data were taken, because the 2.5° × 2.5° NCEP fields fail to resolve variations in precipitation on smaller spatial scales, or because errors exist in the NCEP fields. In the case of the DC94 comparison, we find that the precipitation fields do not exhibit the same trends evident in the deposition bias. In the case of the Fujita et al. (2000) comparison, we remove the effect of differing precipitation fields by considering only concentration. In both cases, errors in the model precipitation field do not fully account for the low model deposition. $NO_x$ emissions from fossil fuel burning, biomass burning, and biogenic sources are all relatively uncertain, and may be too low. The model output is highly dependent on the input emissions, yet characterizing their uncertainty is beyond the scope of this study. The chemistry scheme may underestimate the conversion of $NO_x$ to $HNO_3$, implying an underestimate of hydroxyl (OH) concentrations. However, our sensitivity analysis shows that $HNO_3$ deposition is not very sensitive to the conversion from $NO_x$ to $HNO_3$, and even doubling the implicit OH levels would not eliminate the model's low bias. The very simple model structure may introduce some errors in vertical transport and deposition parameterization, particularly in terms of mixing species away from the boundary layer. Species trapped in the boundary layer may be dry deposited too quickly, rather than being transported downwind in a more realistic manner. The effects of the simple transport scheme in the model are addressed via sensitivity analysis and comparison with a three-dimensional, 11-layer, global Eulerian model, the GFDL GCTM (see Levy et al. (1999)).

Our sensitivity analysis, discussed briefly below, concludes that ATMOS-N is highly sensitive to both wet and dry deposition parameterizations. The comparison (not shown) of GCTM spatial patterns of boundary layer and free-tropospheric concentration fields against those of ATMOS-N indicates that the ATMOS-N produces much less lateral spreading. This spreading in the GCTM reflects the ability of the multi-layer model to capture large-scale transport (although some degree of small-scale spreading in the vicinity of sources would be expected due to numerical diffusion characteristic of Eulerian models). These behaviors may work together to explain a large part of the disagreement between ATMOS-N simulations and observed wet nitric acid deposition. If emissions are trapped in the boundary layer, they could be dry deposited too quickly and not mix up into the upper troposphere for efficient lateral spreading. The excess dry deposition in the model would in turn lead to the exhibited low levels of simulated wet deposition.

### 3.1. Sensitivity analysis

Because a number of model parameters represent simplifications or estimations of physical processes, sensitivity studies were run to assess the impact these uncertain parameters have on model results. These parameters are wet deposition rate ($WD_{HNO_3}$), dry deposition rates ($DD_{HNO_3}$, $DD_{NO_x}$, $DD_{PAN}$), hydroxyl concentrations ([OH]), and Gaussian plume spreading rate.

Table 3 presents SRRs for January in percent and absolute contributions of foreign sources to wet $HNO_3$ deposition in Japan, considering only fossil fuel emissions. The left-hand column gives the January SRRs in the base-case run, with other columns giving the contribution of that source country to Japan's wet $HNO_3$ deposition in the sensitivity runs.

Overall, the percent contributions are quite insensitive to doubling of model parameters. The general patterns and magnitudes of the percent contribution of foreign sources to wet nitric acid deposition do not vary significantly over the range of experiments performed. The absolute values of transport and deposition (also in

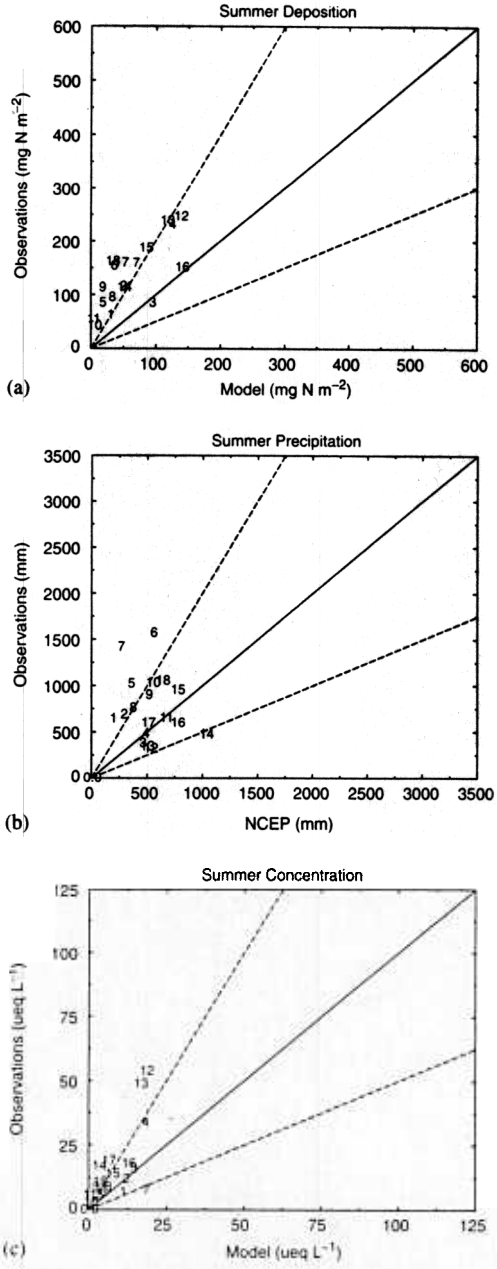


Fig. 8. Summer comparison of $HNO_3$ wet deposition (a), precipitation (b), and concentration (c) between ATMOS-N and Fujita et al. (2000) measurements. Each point represents an observing station, with indices given in Fig. 6b.

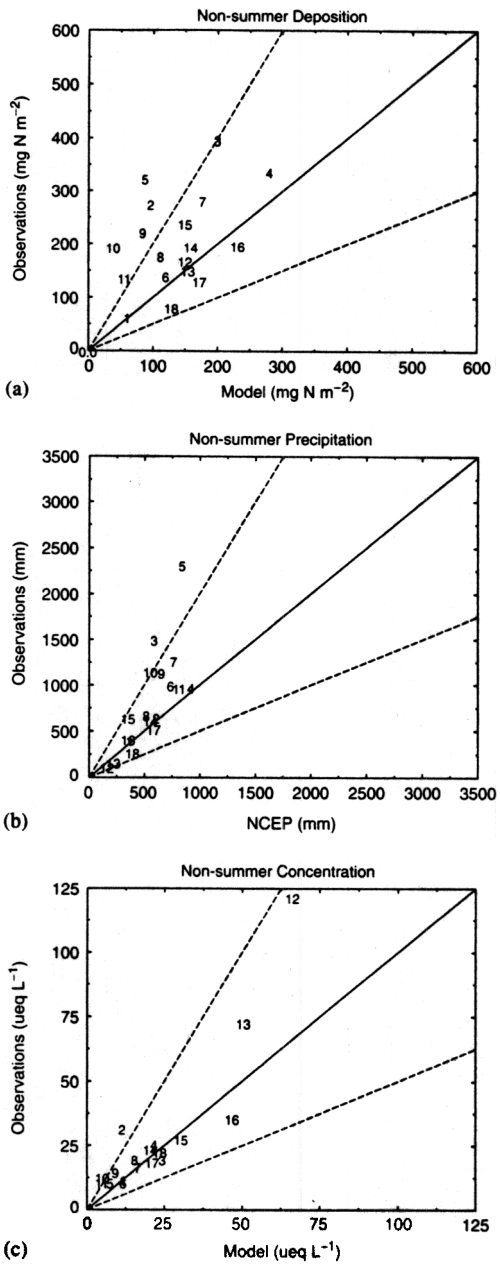


Fig. 9. Same as Fig. 8, for non-summer.

Table 3) are much more sensitive. Doubling dry deposition, for instance, decreases the absolute value of Japan-to-Japan wet nitrate deposition by 20%, whereas the percent contribution stays fixed at 36%. In this case, the enhanced dry deposition rate decreased the Japan–source nitrate deposited as wet deposition, as well as the nitrate available for transport from foreign sources and later wet deposition in Japan. While the relative "blame" of each country is not sensitive to the tested parameter uncertainties, the absolute values of deposition are less robust.

## 4. Results

Tables 4 and 5 summarize the SRRs among east Asian countries, as well as India. Calculations of these SRRs

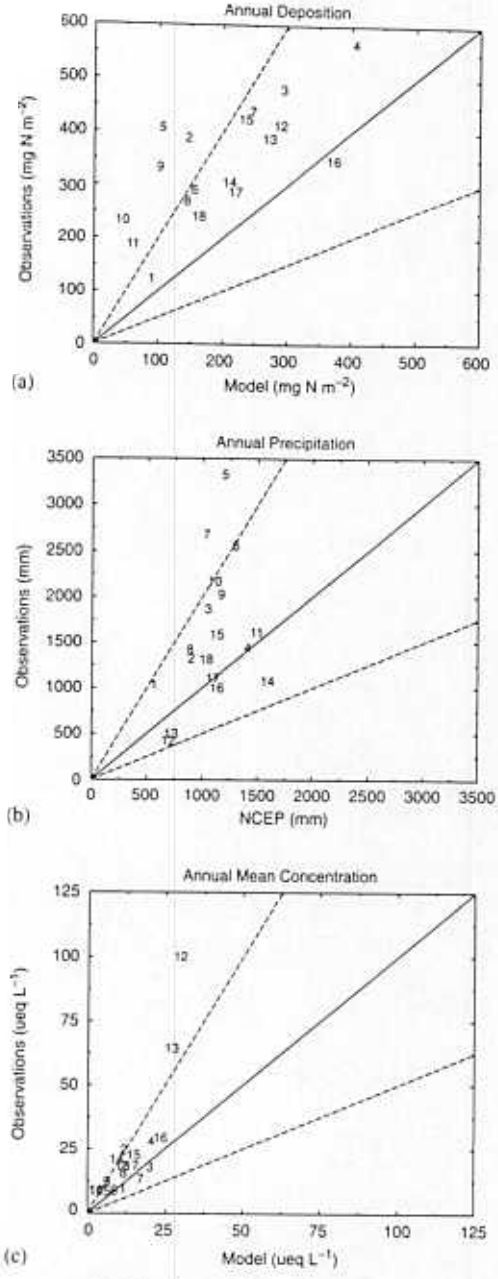


Fig. 10. Same as Fig. 8, for annual.

within ATMOS-N are done on a grid-to-grid basis and include only fossil fuel emissions. The model calculates a matrix of values specifying the contribution of each gridbox's emissions to deposition and concentration values in all other gridboxes. These grid-to-grid values are grouped together to assess SRRs in desired political or geographical domains.

In the tables, each row reports the impact of emissions from the country noted in the left-most column to the total deposition or ambient concentrations in the receptor countries. Values are given in percentage of total deposition/concentration in the receptor country. There are 25 countries within the ATMOS domain, but for clarity we report here only six. Thus, the sum of percentage values in each column often falls short of 100%, due to contributions from other regions within the domain. Total nitrate deposition (Table 4) includes both the locally driven dry deposition and the more long-range transport effects of wet nitric acid deposition. Because wet $HNO_3$ deposition only occurs during precipitation, nitrogen species may be transported far from the emission area before being deposited. Thus, the patterns of long-range transport may be illustrated more clearly by considering wet deposition alone (Table 5).

Of the six nations considered in Table 5, North Korea has the highest relative contribution of imported wet $HNO_3$ deposition. North Korea's fossil fuel emissions are low, and most wind patterns act to import species from North Korea's higher emitting nearby neighbors. South Korea is in a similar position, and thus imports a high fraction of its total wet deposition as well. Due to China's high emission levels and generally upwind position relative to the Korean Peninsula and Japan, China usually contributes the largest percentage of wet deposition due to foreign sources.

The influence of transboundary flow of pollutants on wet $HNO_3$ deposition in Japan exhibits strong seasonal variation, due to the seasonal fluctuations in transport of continental emissions. In the winter and spring, when strong westerly winds carry continental air over Japan and the Pacific, over 50% of wet N deposition in Japan is due to foreign emissions.

The results presented here show that somewhat more transport from China occurs for reactive nitrogen than for sulfur. Ichikawa et al. (1998) estimate that, of the total annual sulfur deposition in Japan, 25% comes from China and 16% from North and South Korea combined. Results from RAINS-Asia, v. 7.52 (calculated using ATMOS by Calori et al., 2001), exhibit similar patterns: 36% of sulfur deposition in Japan from China and 12% from North and South Korea combined. For comparison, this study (Table 4) shows that 18% of fossil-fuel-derived nitric acid deposition in Japan is from emissions in China and 15% from North and South Korea combined.

Although country-wide SRRs for east Asia highlight the major linkages between emissions of $NO_x$ and large-scale nitrate deposition, looking at a single value for an entire country may be misleading. Particularly in China, locally high impacts from foreign emissions may not be reflected in the country total, and even the much smaller Japan has a high degree of inhomogeneity in the distribution of imported versus domestically produced pollution.

Fig. 11 provides an example of the spatial variability of SRRs. Each map depicts the seasonal impact of fossil

Table 3
Wet $HNO_3$ deposition (fossil fuel sources only) deposited on Japan due to emissions from Japan, North Korea, South Korea, and China. Base case compared with sensitivity cases. Both percentage (%) and absolute (kton N month$^{-1}$) values are provided

| | Base case | 2 × Wet dep | 2 × Dry dep | 2 × Growth | 2 × OH |
|---|---|---|---|---|---|
| Percent contribution (%) | | | | | |
| Japan | 36 | 41 | 36 | 37 | 39 |
| N Korea | 4 | 4 | 4 | 5 | 4 |
| S Korea | 15 | 16 | 14 | 15 | 15 |
| China | 41 | 37 | 43 | 41 | 39 |
| Absolute contribution (kton N month$^{-1}$) | | | | | |
| Japan | 4.57 | 6.43 | 3.70 | 4.66 | 5.42 |
| N Korea | 0.54 | 0.61 | 0.43 | 0.59 | 0.59 |
| S Korea | 1.92 | 2.44 | 1.43 | 1.85 | 2.11 |
| China | 5.22 | 5.83 | 4.46 | 5.23 | 5.50 |

Table 4
Annual source–receptor relationships for total $HNO_3$ deposition due to fossil fuel burning. Values given in percentage of total $HNO_3$ deposition in "receptor" countries. "Source" countries listed in left-hand column. "Receptor" countries listed in the top row

| | Emissions (kton N yr$^{-1}$) | Taiwan | Japan | N Korea | S Korea | China | India |
|---|---|---|---|---|---|---|---|
| Taiwan | 116 | **80%** | 2% | | | 2% | |
| Japan | 556 | 1% | **65%** | 1% | 4% | | |
| N Korea | 120 | | 3% | **34%** | 7% | 1% | |
| S Korea | 256 | | 12% | 20% | **63%** | | |
| China | 2132 | 18% | 18% | 46% | 26% | **90%** | |
| India | 1020 | 1% | | | | 6% | |
| Total dep. (kton N yr$^{-1}$) | | 31 | 276 | 66 | 69 | 1173 | 372 |

Table 5
Annual source–receptor relationships for $HNO_3$ wet deposition due to fossil fuel burning. Values given in percentage of total $HNO_3$ deposition in "receptor" countries. "Source" countries listed in left-hand column. "Receptor" countries listed in the top row

| | Emissions (kton N yr$^{-1}$) | Taiwan | Japan | N Korea | S Korea | China | India |
|---|---|---|---|---|---|---|---|
| Taiwan | 116 | **70%** | 2% | | | 2% | |
| Japan | 556 | 1% | **54%** | 1% | 6% | | |
| N Korea | 120 | | 3% | **25%** | 5% | 1% | |
| S Korea | 256 | | 13% | 21% | **51%** | 1% | |
| China | 2132 | 26% | 27% | 53% | 39% | **80%** | |
| India | 1020 | 1% | | | | 12% | |
| Total dep. (kton N yr$^{-1}$) | | 15 | 161 | 35 | 34 | 539 | 188 |

fuel emissions from China, relative to fossil fuel emissions throughout Asia, on wet $HNO_3$ deposition in the region. China exerts the greatest eastward influence in the winter and spring. The contribution of China-derived $HNO_3$ to Japan is largest in northern and southern Japan. In northern Japan, this contribution is primarily due to lack of other significant sources, whereas the high values in southern Japan (70–80% in the spring) reflect the westerly advection from eastern China, where emissions are large. In the summer, the

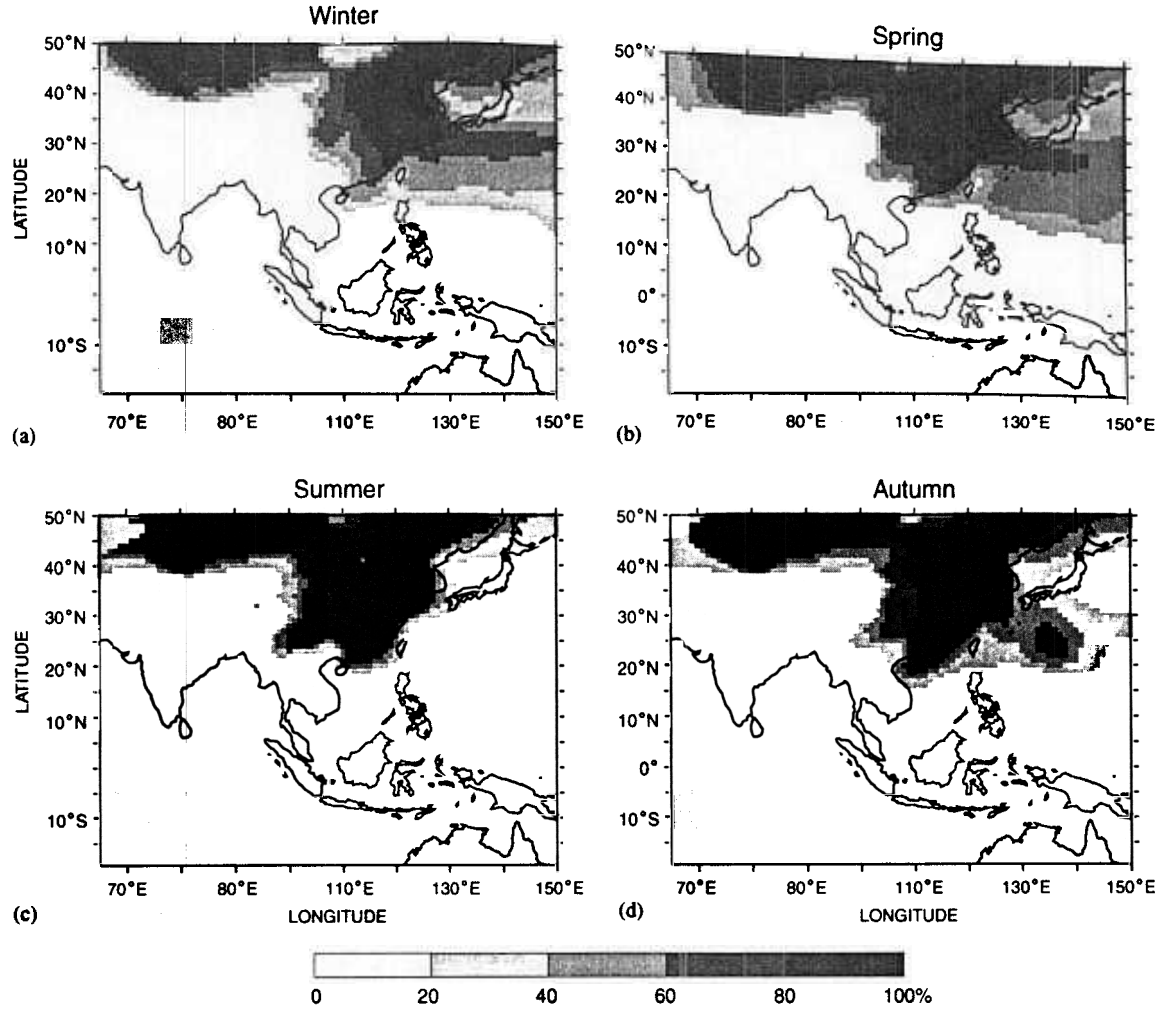


Fig. 11. Percentage (%) impact of fossil fuel emissions from China on nitric acid wet deposition throughout Asia, relative to impact of all regional fossil fuel emissions: (a) winter; (b) spring; (c) summer; and (d) autumn.

gradient of influence is much sharper and closer to the coast, due to both weaker winds and higher precipitation over China.

The significance of the calculated nitrate deposition relationships may be better understood by considering a more complete picture of acid deposition in Asia, combining results for nitrate deposition with those for sulfate deposition. Total acid deposition due to S and N is shown in Fig. 12. Sulfur estimates are taken from simulations with the sulfur-chemistry version of ATMOS (Calori et al., 2001). Results shown here include ATMOS-N simulations with $NO_x$ emissions from fossil fuel burning, biomass burning, and biogenic sources. In the current discussion, only dry and wet $HNO_3$ deposition are assumed to contribute to acidification, which represents a lower bound to acidification from all $NO_y$ species. This assumption leads to at most a 10–15% underestimation of the total acidification due to $NO_y$ deposition, based on the relatively low contributions of $NO_x$ and PAN dry deposition calculated in both ATMOS-N and the GFDL GCTM.

The percentage contribution of nitrate deposition to the total value is mapped in Fig. 13. As expected, the percentage contribution of nitrate is very low in China, where emissions and deposition of sulfur are high. The largest contribution of nitrate is in southeast Asia, where biomass burning is an important source of $NO_x$ emissions. In this area, nitrate contributes 50–90% of the total acid deposition.

Over northern Japan, nitrate deposition accounts for 30–50% of the total acid burden. The importance of sulfate deposition in southern Japan reflects primarily volcanic sources on the south island of Japan. In India, 30–60% of the total acid deposition is due to $NO_x$ emissions.

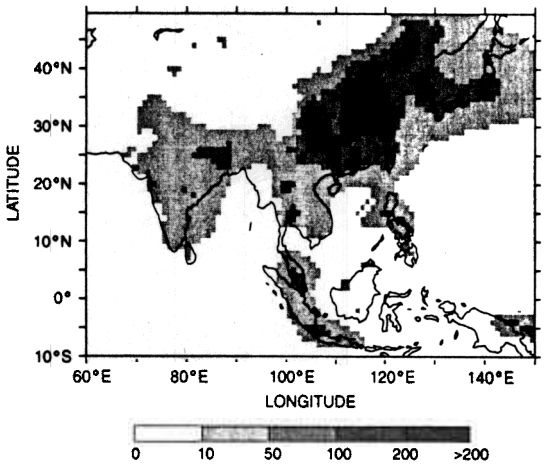


Fig. 12. Annual total acid deposition, due to both sulfate and nitrate (meq $m^{-2} yr^{-1}$).

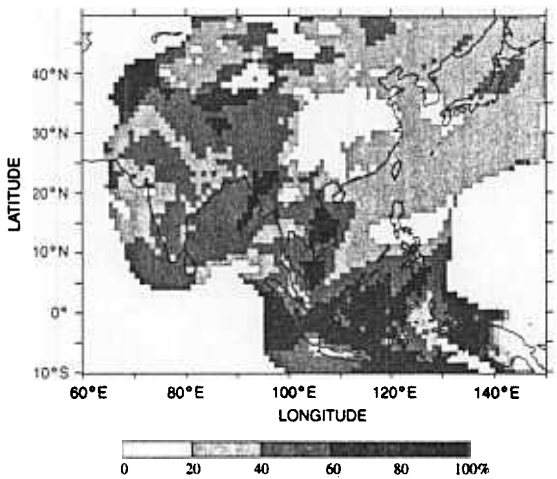


Fig. 13. Percentage (%) contribution of nitrate to annual total acid deposition.

## 5. Summary

Discussion has focused on east Asia and, in particular, the exchange of pollutants among nations. Throughout the region, foreign emissions contribute significantly to domestic budgets of total nitric acid deposition. The influence of long-range transport is particularly important for wet nitrate deposition. In the case of Japan, the most significant foreign source is China, which contributes an annual average of 27% of Japan's wet nitric acid deposition, and 18% of total nitric acid deposition (wet + dry). Although China is a net pollution exporter, regional patterns of influence show that western China is impacted significantly by emissions from India, particularly in the winter.

The Lagrangian "puff" structure of ATMOS-N offers advantages in terms of computational economy and ease in understanding the mechanisms of the simple structure. However, it lacks a realistic treatment of vertical transport, cannot calculate non-linear chemistry, and generally includes more uncertain parameterizations than would be required in a multi-layer model where processes could be approached in a more physically realistic fashion.

This modeling study is intended as an initial, "semi-quantitative" assessment of source–receptor relationships for nitric acid. Results suggest that transport of reactive nitrogen species in Asia should be further investigated with a more realistic three-dimensional chemical transport model.

## Acknowledgements

The authors would like to thank Larry Horowitz, Meredith Galanter Hastings and anonymous reviewers for helpful comments in revising this paper, RAINS-Asia Phase II for support, and Giuseppe Calori for assistance with ATMOS. TAH also thanks the NASA Earth System Science Graduate Fellowship and the Princeton Environmental Institute-Science, Technology and Environmental Policy Program.

## References

Alcamo, J., Shaw, R., Hordijk, L., 1990. The RAINS Model of Acidification: Science and Strategies in Europe. Kluwer Academic Publishers, Boston, MA.

Arndt, R.L., Carmichael, G.R., Streets, D.G., Bhatti, N., 1997. Sulfur dioxide emissions and sectoral contributions to sulfur deposition in Asia. Atmospheric Environment 31, 1553–1572.

Arndt, R.L., Carmichael, G.R., Roorda, J.M., 1998. Seasonal source–receptor relationships in Asia. Atmospheric Environment 32, 1397–1406.

Barrett, K., Seland, O., Foss, A., Mylona, S., Sandnes, H., Styve, H., Tarrason, L., 1995. European transboundary acidifying emissions: ten years calculated fields and budgets to the end of the first sulphur protocol. EMEP/MSC-W, Report 1/95.

Berntsen, T.K., Karlsdottir, S., Jaffe, D.A., 1999. Influence of Asian emissions on the composition of air reaching the north western United States. Geophysical Research Letters 26, 2171–2174.

Calori, G., Carmichael, G.R., 1999. An urban trajectory model for sulfur in Asian megacities: model concepts and preliminary application. Atmospheric Environment 33, 3109–3117.

Calori, G., Carmichael, G.R., Streets, D., Thong boonchoo, N., Guttikunda, S.K., 2001. Interannual variability in sulfur deposition in Asia. Journal of Global and Environmental Engineering 7, 1–6.

Carmichael, G.R., Uno, I., Phadnis, M.J., Zhang, Y., Sunwoo, Y., 1998. Tropospheric ozone production and transport in the springtime in east Asia. Journal of Geophysical Research 103, 10649–10671.

Chameides, W.L., Xingsheng, L., Xiaoyan, T., Xiuji, Z., Chao, L., Kiang, C.S., St. John, J., Saylor, R.D., Liu, S.C., Lam, K.S., Wang, T., Giorgi, F., 1999. Is ozone pollution affecting crop yields in China? Geophysical Research Letters 26, 867–870.

Dentener, F.J., Crutzen, P.J., 1994. A three-dimensional model of the global ammonia cycle. Journal of Atmospheric Chemistry 19, 331–369.

Eliassen, A., 1978. The OECD study of long-range transport of pollutants: long range transport modeling. Atmospheric Environment 12, 479–487.

Foell, W., Green, C., Amann, M., Bhattacharya, S., Carmichael, G., Chadwick, M., Cinderby, S., Haugland, T., Hettelingh, J.-P., Hordijk, L., Kuylenstierna, J., Shah, J., Shrestha, R., Streets, D., Zhao, D., 1995. Energy use, emissions, and air pollution reduction strategies in Asia. Water, Air, and Soil Pollution 85, 2277–2282.

Fujita, S.-I., Takahashi, A., Weng, J.-H., Huang, L.-F., Kim, H.-K., Li, C.-K., Huang, F.T.C., Jeng, F.-T., 2000. Precipitation chemistry in east Asia. Atmospheric Environment 34, 525–537.

Galanter, M., Levy II, H., Carmichael, G.R., 2000. Impacts of biomass burning on tropospheric CO, $NO_x$, and $O_3$. Journal of Geophysical Research 105, 6633–6653.

Galloway, J.N., Dianwu, Z., Jiling, X., Likens, G.E., 1987. Acid rain: China, United States, and a remote area. Science 236, 1559–1562.

Guttikunda, S.K., Thongboonchoo, N., Arndt, R.L., Calori, G., Carmichael, G.R., Streets, D.G., 2001. Sulfur deposition in Asia: seasonal behavior and contributions from various energy sectors. Water, Air, and Soil Pollution 131, 383–406.

Heffter, J.L., 1983. Branching atmospheric trajectory (BAT) model. NOAA Technical Memorandum, ERL ARL-121.

Holloway, T., 2001. Transboundary air pollution in Asia: model development and policy implications. Ph.D. Thesis, Princeton University, Princeton, NJ.

Horowitz, L.W., Jacob, D.J., 1999. Global impact of fossil fuel combustion on atmospheric $NO_x$. Journal of Geophysical Research 104, 23823–23840.

Huang, M., Wang, Z., He, D., Xu, H., Zhou, L., 1995. Modeling studies on sulfur deposition and transport in east Asia. Water, Air, and Soil Pollution 85, 1921–1926.

Ichikawa, Y., Fujita, S., 1995. An analysis of wet deposition of sulfate using a trajectory model for east Asia. Water, Air, and Soil Pollution 85, 1927–1932.

Ichikawa, Y., Hayami, H., Fujita, S.-I., 1998. A long-range transport model for east Asia to estimate sulfur deposition in Japan. Journal of Applied Meteorology 37, 1364–1374.

Jacob, D.J., Logan, J.A., Murti, P.P., 1999. Effect of rising Asian emissions on surface ozone in the United States. Geophysical Research Letters 26, 2175–2178.

Jaffe, D., Anderson, T., Covert, D., Kotchenruther, R., Trost, B., Danielson, J., Simpson, W., Berntsen, T., Kalsdottir, S., Blake, D., Harris, J., Carmichael, G., Uno, I., 1999. Transport of Asian air pollution to North America. Geophysical Research Letters 26, 711–714.

Kasibhatla, P.S., Levy II, H., Moxim, W.J., Chameides, W.L., 1991. The relative impact of stratospheric photochemical production on tropospheric $NO_y$ levels: a model study. Journal of Geophysical Research 96, 18631–18646.

Kasibhatla, P.S., Levy II, H., Moxim, W.J., 1993. Global $NO_x$, $HNO_3$, PAN, and $NO_y$ distributions from fossil fuel combustion emissions: a model study. Journal of Geophysical Research 98, 7165–7180.

Kitada, T., Lee, P.C.S., Ueda, H., 1993. Numerical modelling of long-range transport of acidic species in association with meso-$\beta$-convective-clouds across the Japan Sea resulting in acid snow over coastal Japan—I. Model description and qualitative verifications. Atmospheric Environment 27A, 1061–1076.

Klimont, Z., 2001. Projections of $SO_2$, $NO_x$, $NH_3$ and VOC emissions in east Asia up to 2030. Water, Air, and Soil Pollution 130, 193–198.

Klonecki, A.A., 1998. Model study of the tropospheric chemistry of ozone. Ph.D. Thesis, Princeton University, Princeton, NJ.

Kotamarthi, V.R., Carmichael, G.R., 1990. The long range transport of pollutants in the Pacific rim region. Atmospheric Environment 24A, 1521–1534.

Levy II, H., Moxim, W.J., Klonecki, A.A., Kasibhatla, P.S., 1999. Simulated tropospheric $NO_x$: its evaluation, global distribution, and individual source contributions. Journal of Geophysical Research 104, 26279–26306.

Mauzerall, D.L., Narita, D., Akimoto, H., Horowitz, L., Walters, S., Hauglustaine, D.A., Brasseur, G., 2000. Seasonal characteristics of tropospheric ozone production and mixing ratios over east Asia: a global three-dimensional chemical transport model analysis. Journal of Geophysical Research 105, 17895–17910.

Phadnis, M.J., Carmichael, G.R., 2000. Transport and distribution of primary and secondary nonmethane volatile organic compounds in east Asia under continental outflow conditions. Journal of Geophysical Research 105, 22311–22336.

Simpson, D., 1992. Long-period modelling of photochemical oxidants in Europe. Model calculations for July 1985. Atmospheric Environment 26A, 1609–1634.

Streets, D.G., Carmichael, G.R., Amann, M., Arndt, R.L., 1999. Energy Consumption and acid deposition in northeast Asia. Ambio 28, 135–143.

Ueda, H., Carmichael, G.R., 1995. Formation of secondary pollutants during long-range transport and its contribution to air quality in east Asia. Terrestrial, Atmospheric and Oceanic Science 6, 487–500.

Xu, Y., Carmichael, G.R., 1999. An assessment of sulfur deposition pathways in Asia. Atmospheric Environment 33, 3473–3486.

van Aardenne, J.A., Carmichael, G.R., Levy II, H., Streets, D., Hordijk, L., 1999. Anthropological $NO_x$ emissions in Asia in the period 1990–2020. Atmospheric Environment 33, 633–646.

Wang, Z., Akimoto, H., Uno, I., 2002. Neutralization of soil aerosol and its impact on the distribution of acid rain over east Asia: observed evidence and simulation. Journal of Geophysical Research, in press.

WMO (World Meteorological Organization), 1993. Review of the global precipitation chemistry of BAPMoN, Global Atmosphere Watch, 83.

Yienger, J.J., Levy II, H., 1995. Global inventory of soil-biogenic $NO_x$ emissions. Journal of Geophysical Research 100, 11447–11464.

Yienger, J.J., Galanter, M., Holloway, T.A., Phadnis, M.J., Guttikunda, S.K., Carmichael, G.R., Moxim, W.J., Levy II, H., 2000. The episodic nature of air pollution transport from Asia to North America. Journal of Geophysical Research 105, 26931–26945.